Radiation Transport

G. Magelssen

July 1977

UWFDM-215

FUSION TECHNOLOGY INSTITUTE

UNIVERSITY OF WISCONSIN

MADISON WISCONSIN

Radiation Transport

G. Magelssen

Fusion Technology Institute
University of Wisconsin
1500 Engineering Drive
Madison, WI 53706

http://fti.neep.wisc.edu

July 1977

UWFDM-215

Radiation Transport Within Laser Fusion Targets

Glenn Magelssen

UWFDM-215

July 1977

Fusion Technology Program
Nuclear Engineering Department
University of Wisconsin
Madison, Wisconsin 53706

I. Introduction

Radiative processes and transport can play an important role in the compression and heating of a fusion pellet irradiated by a laser beam. In order to achieve densities high enough for efficient thermonuclear burn, the fusion pellet must be compressed along a low adiabat[1]. This will not be possible if the compressed region of the pellet is significantly preheated by X-rays originating in the hot outer regions[2]. Further, radiation flow and energy loss during implosion and burn can influence the ion and electron fluid motion and energy and, thus, the implosion and burn process.

Because reactor wall damage may depend upon the X-ray spectra and energy leaving the pellet, radiation could also play a significant role in the design of the laser fusion reactor. The X-ray spectra and energy escaping a pellet will depend upon its design. For example, the X-ray spectra leaving the pellet, the transit time to the wall,and the energy content will change with the design of the pellet.

In this report, the results of numerical calculations of the solution to the coupled hydrodynamics, burn dynamics and radiation transport equations for a bare DT pellet and for a DT pellet surrounded by a layer of mercury are presented. The implosion calculation is not done. Consequently, initially, the pellet is assumed to be in a given compressed state. The purpose of this report is threefold. It is to outline the physics assumed in the numerical calculations and to describe the technique used to solve the radiation transport equation. Most importantly, it is to discuss the relationship of radiation transport to thermonuclear burn and hydrodynamic motion.

Sections II, III and IV describe and discuss, respectively, the hydrodynamics, burn dynamics and radiation processes. Section V gives a detailed discussion of the radiation transport method and Section VI contains our results and a discussion of the important interconnected physical processes. Special effects resulting fron neutron and alpha particle transport are described in Section VII.

II. Hydrodynamics

1. Introduction

Since one of the purposes of this report is to emphasize the radiation transport aspect of the laser-pellet physics, other areas of the problem are only briefly described. A more complete discussion will be given in a later report.

To understand in detail the dynamics and interaction of laser light heating, thermal conduction, ablative-implosion and thermonuclear burn, the laser fusion plasma is typically modeled using the hydrodynamics description along with non-hydrodynamic laser-plasma interaction physics and rate equations to predict thermonuclear yield.[3] Solution of the hydrodynamics equations generally requires that the plasma be in local thermodynamic equilibrium (LTE) where equations of state and transport coefficients can be defined to close the set of equations.[4] This is generally valid for a collision dominated dense plasma, although there are important exceptions that can strongly alter the results given by a purely hydrodynamic description (thermonuclear reaction product charged particles, photons, and nonthermal electrons).

2. Two Temperature One Fluid Model

For the purposes of modeling pellet implosions and thermonuclear burn, a one fluid two temperature plasma hydrodynamics model is used. Thus, electrons and ions are assumed to move together as a single fluid

(with the same velocity) implying charge neutrality. For purposes of energy transfer, the electrons and ions are treated as separate species, each in local thermodynamic equilibrium at different temperatures, T_e and T_i.

The one fluid two temperature hydrodynamic equations used in our calculations can be written:

$$\frac{\partial \rho}{\partial t} + \nabla \cdot (\rho \underline{u}) = 0 \tag{1}$$

$$\rho \left[\frac{\partial \underline{u}}{\partial t} + \underline{u} \cdot \nabla \underline{u} \right] = - \underline{\nabla} (P_e + P_i + P_r) \tag{2}$$

$$\rho C_{v_e} \left[\frac{\partial T_e}{\partial t} + \underline{u} \cdot \underline{\nabla} T_e \right] = \underline{\nabla} \cdot K_e \underline{\nabla} T - P_e (\underline{\nabla} \cdot \underline{u}) \tag{3}$$

$$- \omega_{ei} (T_e - T_i) + S_e$$

$$\rho C_{v_i} \left[\frac{\partial T_i}{\partial t} + \underline{u} \cdot \underline{\nabla} T_i \right] = \underline{\nabla} \cdot K_i \underline{\nabla} T_i - P_i (\underline{\nabla} \cdot \underline{u}) \tag{4}$$

$$+ \omega_{ei} (T_e - T_i) + S_i$$

One must have equations of state to close this set of equations

$$P_e = P_e(n_e, T_e) \quad ; \quad P_i = P_i(n_i, T_i)$$

$$C_{v_e} = C_{v_e}(n_e, T_e) \quad ; \quad C_{v_i} = C_{v_i}(n_i, T_i)$$

The transport law for the heat fluxes q_c and q_i has already been specified in the form of Fourier's law:

$$q_e = -K_e \nabla T_e \qquad q_i = -K_i \nabla T_i$$

so that expressions must also be supplied for the transport coefficients:

K_e - electron thermal conductivity

K_i - ion thermal conductivity

ω_{ei} - electron-ion temperature equilibration coefficient

The forms of these terms will be discussed in the next two sections. Along with convection, conduction, work and equilibration terms, each temperature equation has an external source term. The electron source term will account for temporal and spatial electron energy gain and loss with the nonthermal radiation field; energy gain from the absorption of laser light; and gain from the redeposition of energy by non-thermal thermonuclear reaction products. The ion source must account for gain from thermonuclear reaction product energy redeposition.

With the annihilation of ions by fusion reactions and the treatment of the resultant reaction products as separate non-hydrodynamic species, the right hand side of the continuity equation must strictly be replaced by annihilation and creation terms to account for fusion reactions and rethermalization of reaction products.

3. Equation of State

The equations of state for a relatively hot, fully ionized plasma can be adequately approximated by the ideal gas laws.

$$P_e = n_e k_e T_e \quad , \quad P_i = n_i k_B T_i \tag{5}$$

$$C_{v_e} = 3/2\ k_B\ Z/m_i, \quad C_{v_i} = 3/2\ k_B/m_i \tag{6}$$

Unfortunately, the cold, highly compressed DT and mercury plasmas ahead of the converging shock fronts during implosion do not obey this law. The electrons are Fermions and strictly obey Fermi-Dirac rather than Boltzmann statistics.[7]

In this highly compressed, cold state they begin to fill all the available low energy states and equations of state must be derived from Fermi-Dirac distribution functions.[5] In addition, the energy associated with different solid phases, the liquid phase, dissociation and ionization of pellet materials must be treated in order to correctly predict the electron pressure. For high Z materials the differing ionization states must also be treated, even at high temperatures, through models such as Saha or Coronel equilibrium or by solving the non-equilibrium ionization rate equations. These complications require different theories and approximations for each temperature and density range and for every different material. A great amount of theoretical and experimental work has been invested in accurate equations of state in support of the nuclear weapons program , and more recently directly in support of the needs of the laser fusion effort. Equations of state for purposes of computation are usually in the form of tables of pressure values and tables of fitting parameters that are evaluated to obtain pressure values as functions of density or compressibility and temperature.

In the work presented here the equation of state aspect to the pellet problem is greatly simplified to obtain some qualitative results. To find a rough estimate of the pellet dynamics, particle and X-ray spectra, the ideal gas laws are assumed to be valid for the high Z material. The state of ionization is approximated by equilibrating ionization change with temperature change where LTE estimates of ionization stages are used. The rate of ionization is assumed instantaneous compared to the hydrodynamic time scale. Recombination is assumed to be collisional (three body) and electron energy losses by ionization and gain by recombination are included in the electron source term. In the future tables which contain more accurate information about the LTE plasma equation of state will be available. Since

there is very little published information on radiation transport within tamped pellets, this additional information will enable us to make a more quantitative comparison with the qualitative results presented in this report.

4. Transport Coefficients

a. Particle

The transport coefficients in our model are given by the classical values (Spitzer).[7]

$$K_e = \frac{20(\frac{2}{\pi})^{3/2} k_B (k_B T_e)^{5/2}}{m_e^{1/2} e^4 Z \ln\Lambda_{ei}} \tag{7}$$

$$K_i = \frac{20(\frac{2}{\pi})^{3/2} k_B (k_B T_i)^{5/2}}{m_i^{1/2} e^4 Z^4 \ln\Lambda_{ii}} \tag{8}$$

$$\omega_{ei} = \frac{8(2\pi)^{1/2} n_e Z^2 e^4 \ln\Lambda_{ei}}{3 m_e m_i k_B^{3/2}} \left(\frac{T_e}{m_e} + \frac{T_i}{m_i}\right)^{-3/2} \tag{9}$$

Because the laser heats the electrons, the electron heat flux can be very strong, resulting in very steep temperature gradients that apparently violate the hydrodynamic criteria

$$T_e/\nabla T_e < \lambda_e$$

where λ_e is the electron mean free path. The result of this breakdown of the transport law is an electron thermal wave propagation speed far in excess of the electron thermal velocity; a clearly nonphysical result. To avoid this problem, an electron thermal flux limiter has been added to the temperature equations[8]

$$q_e = - K_e \nabla T_e = \frac{- k_e \nabla T_e}{1 + \frac{K_e \nabla T_e}{(q_{max})}} \qquad (10)$$

where q_{max} is an upper limit on the physically achieveable heat flux which is usually dependent on local electron density and temperature.

In the previous discussion, the other major transport coefficient, viscosity, has been ignored. Laser fusion plasmas are generally treated as an inviscid fluid although the equation of motion for such a fluid becomes purely hyperbolic and admits discontinuous solutions such as shocks. Such discontinuities are very difficult to treat numerically so that artificial viscosity is empirically introduced into the hydrodynamics equations in the form of an additional pressure[9]

$$P_i \rightarrow P_i + q$$

that is zero everywhere except in the vicinity of a shock, where it adds dissipation. Our model uses an artificial viscosity such that the jump conditions across the shock are preserved.

III. Burn Dynamics

a. Reaction Rates

Consider the most reactive fusion fuel, a 50-50 atomic mixture of deuterium and tritium, the two heavy isotopes of hydrogen. They fuse to form a helium nucleus (alpha particle) and a neutron[15].

$$_1D^2 + {}_1T^3 \rightarrow {}_2H_e^4 \ (3.5 \text{ MeV}) + {}_0n^1 \ (14.1 \text{ MeV})$$

The energy released in this reaction (Q-value) is approximately 17.6 MeV with 3.5 MeV going to the charged alpha particle. The reaction rate for thermonuclear D-T fusion $(\overline{\sigma v})_{DT}$ is plotted in Figure 1. The next most probable reaction is between two deuterium nuclei.

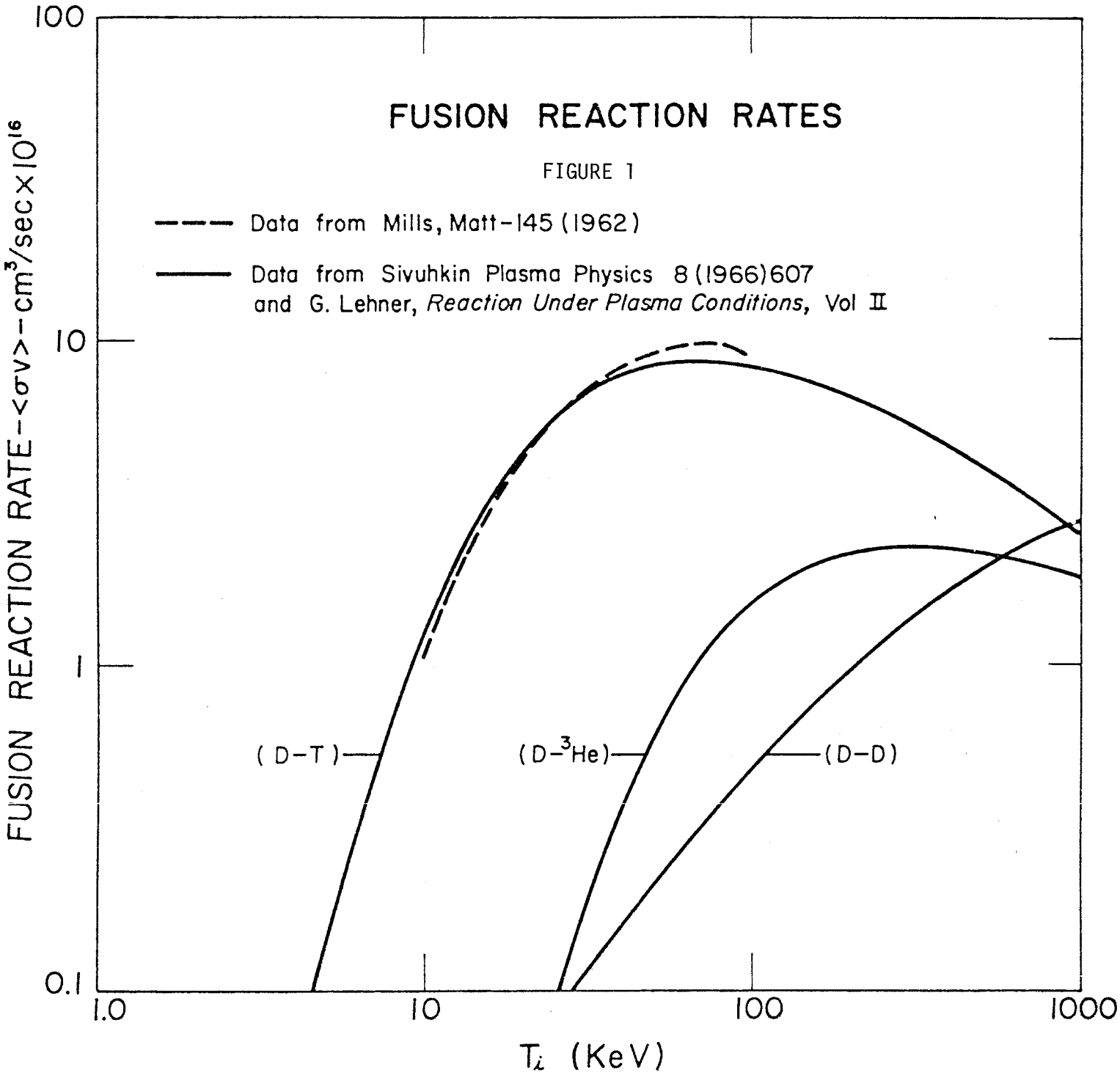
FUSION REACTION RATES
FIGURE 1
Data from Mills, Matt-145 (1962)
Data from Sivuhkin Plasma Physics 8 (1966) 607
and G. Lehner, Reaction Under Plasma Conditions, Vol II
FUSION REACTION RATE - $\langle\sigma v\rangle$ - $cm^3/sec \times 10^{16}$
100
10
1
0.1
1.0
10
100
1000
T_i (KeV)
(D-T)
(D-^{3}He)
(D-D)

$$ {}_1D^2 + {}_1D^2 \xrightarrow{50\%} {}_2He^3\ (.82\ MeV) + {}_0n^1\ (2.45\ MeV) $$

$$ \xrightarrow{50\%} {}_1T^3\ (1.01\ MeV) + {}_1P^1\ (3.02\ MeV) $$

The average Q-value is 3.15 MeV while the average energy going into charged particles is 1.925 MeV. The D-D fusion reaction rate $(\overline{\sigma v})_{DD}$ is also plotted in Figure 1.

In our model are the rate equations for thermal deuterium and tritium concentrations. They are:

$$ \frac{dn_D}{dt} = - n_D n_T\ (\overline{\sigma v})_{DT} - n_D^2\ (\overline{\sigma v})_{DD} \qquad (11) $$

$$ \frac{dn_T}{dt} = - n_D n_T\ (\overline{\sigma v})_{DT} \qquad (12) $$

Because the DD reaction produces a tritium ion for every two fusions it would seem that the equation for n_T should contain a positive term proportional to $n_D^2\ (\overline{\sigma v})_{DD}$. The tritium ion reaction product is not thermal however, and must be treated separately because its "beam plasma" reaction rate is much greater than the Maxwellian averaged thermal reaction rate.
For the calculations presented the DD reaction process is ignored because its contributions to the eventual energy deposition and loss are negligible compared to the DT reaction products for the temperature and densities considered.

b. Charged Particle Transport

Particular attention has been drawn to the energy of the charged particle reaction products. The requirement for efficient thermonuclear burning is that the range of the charged particle reaction products is a small fraction of the radius of the dense pellet core. In this way, only a small central

hot spot need be heated to an ignition temperature, 4-10 KeV. Once burning starts, the reaction product energy redeposition will quickly "bootstrap" heat the microcore to greater than 20 keV where the D-T reaction rate is greatest. As the hot microcore becomes transparent to the reaction products they stream out and are rapidly thermalized in the surrounding colder plasma. In this way a thermonuclear detonation wave propagates outward from the microcore. A useful way to visualize this process is to imagine a burning log. In this case the hot region occurs at the surface and the burn wave propagates inward toward the log's core.

To accurately describe the thermonuclear burn process one must not only solve the rate equations but must treat the transport and thermalization of the reaction products. Our model is to use the Fokker-Planck equation for a fast test particle in a thermal background plasma to obtain a range-energy relation. It is [10]:

$$\frac{dv}{ds} = - 4\pi\, r_o^2\, m_e^2\, n_i\, Z_i^2\, Z^2\, \ln\Lambda_i^i / m_i m\, v^3 \; - \qquad (13)$$

$$4\,(2\pi)^{1/2}\, r_o^2\, m_e^{5/2}\, n_e\, Z^2\, \ln\Lambda_e^e / 3m\,(k_B T_e)^{3/2}$$

where r_o is the classical electron radius, and the unsubscripted variables apply to the fast charged particles. The two terms for slowing down in electrons and ions are plotted in Figure 2 . The energy loss rate to electrons is independent of the fast particle velocity; however, the energy loss rate to ions increases as the fast particle velocity decreases. Thus, in a fully ionized DT mixture the particles lose most of their energy to electrons along the first part of their path and to the ions near the end of their flight. The charged particle transport technique used in our analysis will be described in a later report.

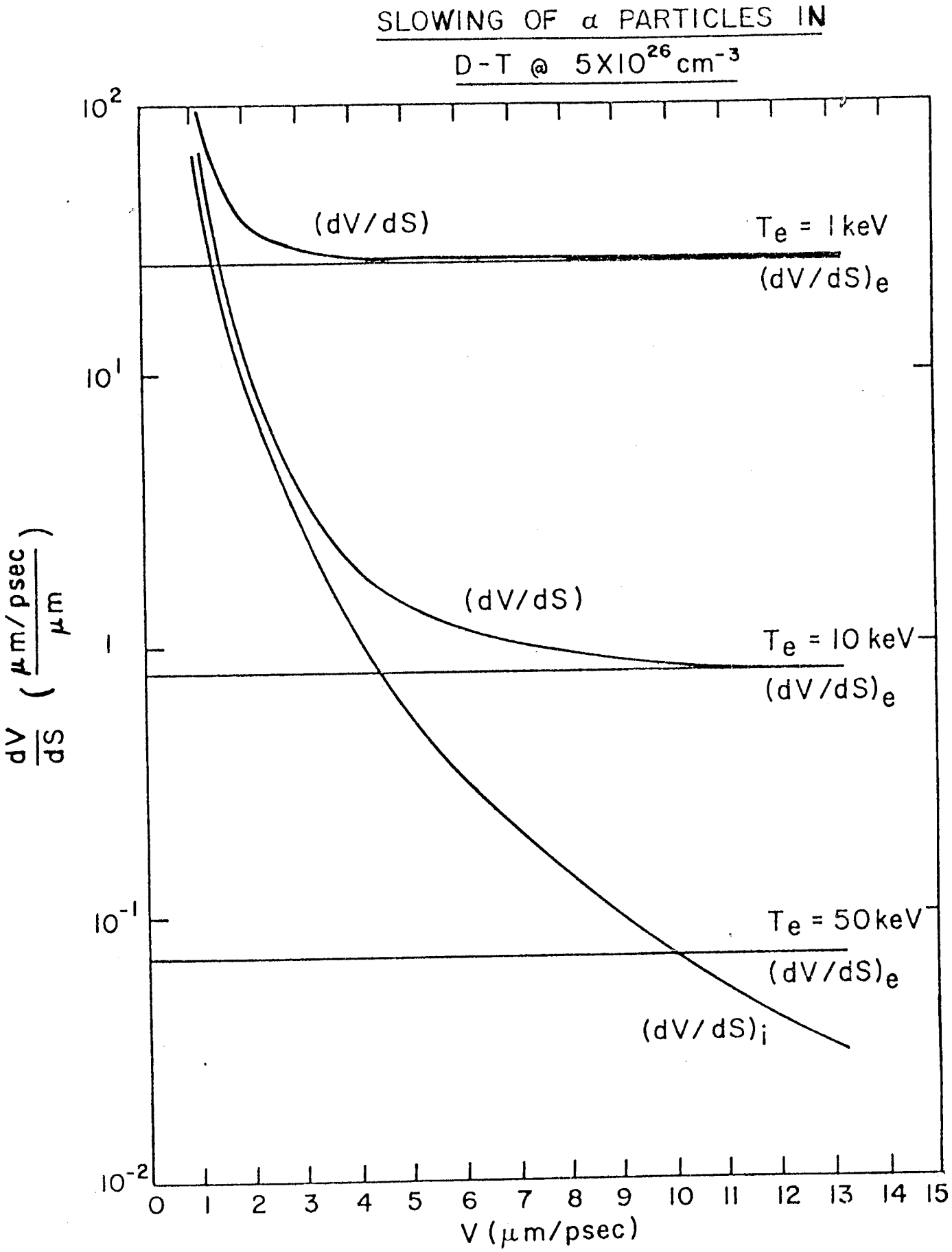
SLOWING OF α PARTICLES IN
D-T @ 5X10^26 cm^-3
10^2
10^1
1
10^-1
10^-2
dV/dS (μm/psec / μm)
(dV/dS)
Te = 1 keV
(dV/dS)e
(dV/dS)
Te = 10 keV
(dV/dS)e
Te = 50 keV
(dV/dS)e
(dV/dS)i
0 1 2 3 4 5 6 7 8 9 10 11 12 13 14 15
V (μm/psec)

FIGURE 2

For certain conditions of temperature and density the above model may overestimate the energy-range of charged particles. For example, it is implicitly assumed in this analysis that charge neutrality exists and that collective electric field fluctuations do not. The existence of such fields could cause the charged particles to slow down more quickly than estimated by the Fokker-Planck model. Some of the physical implications of this increased slowing down are discussed in section VII. The charged particle slowing down in the background plasma acts as a source of both energy and momentum and as such the particles affect the hydrodynamic behavior of the plasma. The hydrodynamics in turn affects the temperature and density so that the hydrodynamics and burn dynamics must be treated as coupled processes.

c. Neutron Transport

It has been suggested that neutron scattering within pellets with ρrs as large as those considered in this report will have important consequences on pellet dynamics. Because neutrons carry a large amount of energy, any significant energy loss (i.e. 10% or more) within the pellet will act as a large energy input into the plasma. Because neutrons have large mean free paths their net effect will be one of plasma heating. This increased heating could quicken the disassembly of the pellet and possibly change the fractional burnup, yield and gain. As a first approximation neutrons are assumed not to scatter within the pellet, and therefore, a neutron transport calculation is not done. The significance of this assumption on radiation transport is discussed in section VII.

VI. Radiation Processes

A simple model of the emission and absorption processes is used. In the future tables containing more accurate information will be employed in the calculation. Only thermal bremsstrahlung emission and inverse bremsstrahlung absorption are considered. The bremsstrahlung emission into 4π steradians is given by:[2]

$$J_{ff}(v)dv = 8.05 \cdot 10^{-46} \frac{N_e N_i}{\sqrt{kT_e}} \Sigma C_z Z_1^2 e^{-\frac{hv}{kT}} g_{ff}\, dv \text{ ergs/cm}^3\text{-sec}$$

where C_z is the concentration of atomic element Z_i; Z_1 is the mean ion charge of element Z_i; N_e and N_i are the electron and ion number densities and g_{gg} is the Gaunt factor averaged over a Maxwellian velocity distribution. The Born approximation is used and the Gaunt factor is written as:

$$g_{ff} = \frac{\sqrt{3}}{\pi} k_o(x)\, e^x$$

where $$x = hv/2kT_e$$

and where $k_o(x)$ is given in terms of the modified Bessel function of imaginary argument

$$K_o(x) = \pi/2\, [i\, H_o(x)]$$

Absorption coefficients corrected for induced emission are obtained from the emission function by Kirchoff's law,

$$\sigma(v) = \frac{J(v)}{B(v)} = \frac{(hc)^2}{2} \frac{J(v)}{(hv)^3} \left(e^{\frac{hv}{kT}} - 1\right)$$

where $J(v)$ is the bremsstrahlung emission function J_{ff}. Thomson scattering for free electron at rest is assumed.

Recombination and line emission and their absorption counterparts are important processes for high Z materials. Because only very rough estimates of the X-ray and charged particle spectra and energy contents are wanted and because only very general relationships between burn, radiative transport and hydrodynamic motion are sought, these processes are neglected.

V. Radiation Transport

1. Introduction

To solve the radiation transport problem the relationship between radiative specific intensity and other physically meaningful quantities needs to be determined. In terms of the specific intensity the energy density at a given frequency is

$$E(\underline{r},v,t) = 1/c \int_{4\pi} d\underline{r}\ I(\underline{r},v,\underline{\Omega},t) \tag{14}$$

the i-th component of the radiation flux vector is

$$F_i(\underline{r},v,t) = \int_{4\pi} d\underline{r}\ \Omega_i\ I(\underline{r},v,\underline{\Omega},t) \tag{15}$$

and the ij-th component of the radiative pressure tensor is

$$P_{ij}(\underline{r},v,t) = \int_{4\pi} d\underline{\Omega}\ \Omega_i\ \Omega_j\ I(\underline{r},v,\underline{\Omega},t) \tag{16}$$

These are the variables used in our radiation transport model.

After making certain assumptions about the radiation and its interaction with matter, the radiative specific intensity can be shown to satisfy a continuity equation of the form[11]

$$\begin{aligned} 1/c\ \frac{\partial}{\partial t}\ I(r,\underline{\Omega}) &= -\ \underline{\Omega} \cdot \underline{\nabla}\ I(v,\underline{\Omega}) \\ &- \sigma_a(v)\ I(v,\underline{\Omega}) + J(v)\ (1 + c^2\ I(v,\underline{\Omega})/2hr^3) \\ &- \int\int dv'\ d\underline{\Omega}'\ \sigma_s\ (v\rightarrow v',\ \underline{\Omega} \cdot \underline{\Omega}')\ I(v,\underline{\Omega})\ \ (1 + \frac{c^2\ I(v',\underline{\Omega}')}{chv'^3}) \\ &+ \int\int dv'\ d\underline{\Omega}'\ \sigma_s\ (v'\rightarrow v,\ \underline{\Omega} \cdot \underline{\Omega}')\ \frac{v}{v'}\ I(v',\underline{\Omega}')\ (1 + \frac{c^2\ I(v,\underline{\Omega})}{2h_v^3}) \end{aligned} \tag{17}$$

where the first term on the right hand side of the equation is due to photon streaming, the second to photon absorption, the third to photon emission, the fourth to photon outscattering ($\nu \to \nu'$ and $\underline{\Omega} \to \underline{\Omega}'$) and the last to photon inscattering ($\nu \to \nu'$ and $\underline{\Omega}' \to \underline{\Omega}$).

A discussion of the variable Eddington method, the method used to solve the transport equation, is given in the next section. This method is based on the expansion of the angular moments $\int I u^k du$ for one dimensional planar or spherical symmetric problems. The expansion is truncated after the second moment and a semiempirical expression is used to determine the pressure tensor.

The variable Eddington method was chosen for four basic reasons. First, the method gives energy and spectral X-ray information -- information which may be necessary for the design of the laser-fusion reactor. Second, the technique can treat plasmas with both large and small opacities. This requirement is necessary because radiative mean free paths can be much larger and much smaller than the pellet size. Third, it limits to the correct physical equations -- the streaming form for long and the diffusive form for short mean free paths. Finally, the method is computationally inexpensive. Because the number of time iterations for a hydrodynamical burn calculation is large, the technique should not require an excessive amount of cost per time cycle.

2. Variable Eddington Method

a. Introduction

For problems with one dimensional symmetry the specific intensity at a given frequency can be defined in terms of its position r, its direction cosine with respect to r, μ, and the time t. The results of the previous section illustrate that the radiation energy density, flux and pressure can be obtained from the specific intensity. The radiation energy density at a given frequency is

$$E(\nu, r, t) = \frac{2\pi}{c} \int_{-1}^{1} I(\nu, r, \mu, t)\, d\mu \qquad (18)$$

The r component of the radiative flux is

$$F(\nu, r, t) = 2\pi \int_{-1}^{1} I(\nu, r, \mu, t)\, \mu d\mu \qquad (19)$$

and the rr component of the radiation pressure is

$$P(\nu, r, t) = \frac{2\pi}{c} \int_{-1}^{1} I(\nu, r, \mu, t)\, \mu^2 d\mu \qquad (20)$$

For planar or spherical symmetry the continuity equation (eq.17) can be written as[12]

$$\frac{1}{c}\frac{\partial I}{\partial t} + \mu\frac{\partial I}{\partial r} + 1/2\ (\alpha - 1)\ \frac{(1 - \mu^2)}{r}\frac{\partial I}{\partial \mu} +$$

$$(\sigma_a + \sigma_s)\ I = J/4\pi + S \qquad (21)$$

where $\alpha = 1$ for plane and $\alpha = 3$ for spherical geometry. Notice that in writing this equation coherent scattering is assumed. If there is no change in frequency upon scattering (coherent scattering) induced inscattering and outscattering terms cancel. The functional structure of the absorption and scattering cross sections (σ_a and σ_s) and the emission and scattering source functions (J and S) depend on the atomic model and the chemical content of the plasma. For the plasmas considered, low temperature (several kilovolts) and fluid velocities much less than the speed of light,

$$S(\nu, r, \mu, t) = \sigma_s \int_{-1}^{1} K(\mu,\mu')\ I(\nu, r, \mu', t)\, d\mu' \qquad (22)$$

where $K(\mu,\mu')$ is assumed the Thomson scattering kernal for free electrons at rest[13]. Thus,

$$K(\mu,\mu') = 1/2\ [1 + (3\mu^2 - 1)\ (3\mu'^2 - 1)]\ . \qquad (23)$$

Even though the complexity of the transport equation is considerably reduced by these approximations, it is still extremely difficult to solve in its present form. Our approach is to assume that the angular distribution of the radiation is not a critical quantity. The transport problem can then be simplified by eliminating the direction cosine. The variable Eddington method is based on an expansion of the angular moments $\int I(\nu, r, \mu, t)\ \mu^k\ d\mu$.[14] Using equation (21), the first two moments are

$$\frac{\partial E}{\partial t} + \frac{1}{r^{\alpha - 1}}\ \frac{\partial}{\partial r}\ (r^{\alpha - 1}\ F) + c\ \sigma_a\ E = J \qquad (24)$$

$$\frac{1}{c}\ \frac{\partial F}{\partial t} + c\ \left[\frac{\partial P}{\partial r} + \frac{\alpha-1}{r}\ (3P - E)\right] +$$

$$(\sigma_a + \sigma_s)\ F = 0 \qquad (25)$$

Notice that μ has been eliminated and that the frequency appears only as a parameter. Notice also, however, that there are three dependent variables and only two equations. In a moment representation each equation contains at least one higher order moment. In the variable Eddington technique only the first two equations of the moment expansion are kept and one must develop a semiempirical expression for the pressure tensor,

$$P = f\ E \qquad (26)$$

where $f = f(v, r, t)$ is called the Eddington factor. If the correct form of the Eddington factor were known this method would be equivalent to the full transport equation. In practice only approximate expressions for f are used which are based on a simple physical model. The primary requirement on f is that it should limit to a value of 1/3 in regions with large opacities (isotropic radiation) and to a value of 1 in regions with small opacities (streaming radiation).

b. Diffusion and Streaming Limits

The variable Eddington technique has the necessary property of limiting to wave propagation in optically thin regions and to diffusion transport in optically thick regions. To see this consider the plane geometry case.

For plane geometry equations (24) and (25) become

$$\frac{\partial E}{\partial t} + \frac{\partial F}{\partial r} + c\,\sigma_a\,E = J$$

$$1/c\,\frac{\partial F}{\partial t} + c\frac{\partial}{\partial r}\,(fE) + (\sigma_a + \sigma_s)\,F = 0$$

or an optically thick region

$$1/c\,\frac{\partial F}{\partial t} \ll (\sigma_s + \sigma_a)\,F$$

This implies that

$$F \approx -\,c/(\sigma_a + \sigma_s)\;\frac{\partial\,(fE)}{\partial r}$$

In addition, for an optically thick region $f \to 1/3$; therefore

$$F \approx -\,c/3(\sigma_a + \sigma_s)\,\frac{\partial E}{\partial r}$$

This expression is the familiar form for the flux in a diffusive medium. Using this expression for the flux and using the energy equation, the diffusion form of the transport equations can be written as

$$\frac{\partial E}{\partial t} - \frac{\partial}{\partial r}\left(\frac{c}{3(\sigma_a + \sigma_s)}\frac{\partial E}{\partial r}\right) + c\,\sigma_a E = J$$

This is the nonLTE diffusion form of the radiation transport equation. For optically thin regions $\sigma \to 0$. In this limit equations (24) and (25) become

$$\frac{\partial E}{\partial t} + \frac{\partial F}{\partial r} \simeq 0$$

$$1/c\,\frac{\partial F}{\partial t} + c\,\frac{\partial E}{\partial r} \simeq 0$$

Notice that the Eddington factor has been set equal to one, its free streaming value. Eliminating F yields:

$$\frac{\partial^2 E}{\partial t^2} + c^2\,\frac{\partial^2 E}{\partial r^2} = 0$$

which is just the wave equation for photons.

c. The Eddington Factor

A simple physical model is used to determine the Eddington factor. The primary criterion on f is that it limit to the correct physical values. For example, f must limit to 1/3 for optically thick and to 1 for optically thin regions of the plasma. Consider the vacuum region, the annular region between the two radiating concentric spheres shown in Figure 3.[13] The sphere near the origin is denoted by 1 while the outer sphere is denoted by 2.

Figure 3

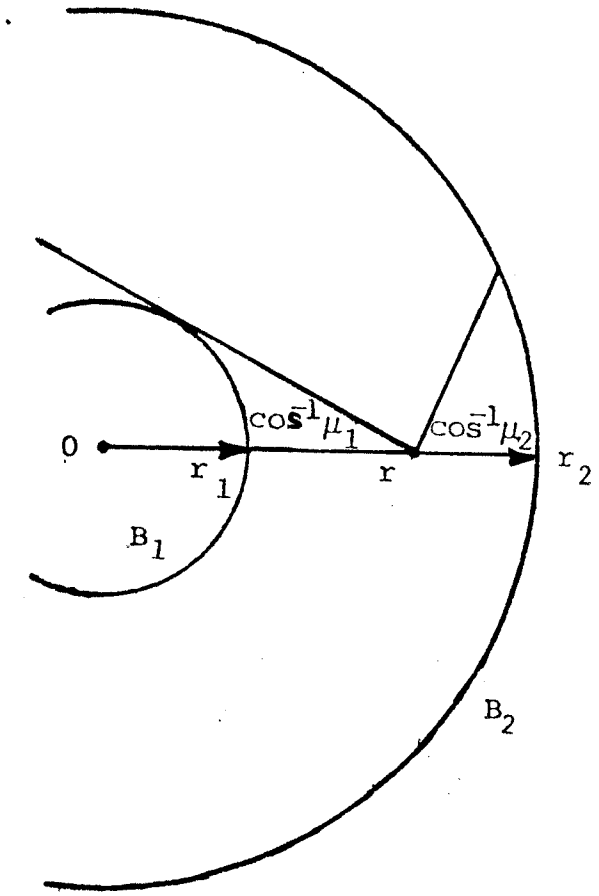

Eddington Factor Model of Vacuum Region
between Two Concentric Radiating Spheres

Geometry is used to calculate μ_1 and radiation retardation to calculate μ_2.[13]

The expressions for E, F and P are

$$\mu_2 < 0 \qquad E = \frac{2\pi}{c}\left[B_1(1-\mu_1) + B_2(1+\mu_2)\right] \tag{27}$$

$$F = \pi\left[B_1(1-\mu_1^2) - B_2(1-\mu_2^2)\right] \tag{28}$$

$$P = \frac{2\pi}{3c}\left[B_1(1-\mu_1^3) + B_2(1+\mu_2^3)\right] \tag{29}$$

where B_1 is the radiation source for sphere 1 while B_2 is the source for sphere 2. Therefore,

$$f = P/E = 1/3\left[1 + \frac{2F}{cE}(\mu_1+\mu_2) - \frac{2\pi\,\mu_1\,\mu_2}{cE}\left[\frac{B_1}{\mu_1}(1-\mu_1^2) - \frac{B_2}{\mu_2}(1-\mu_2^2)\right]\right] \tag{30}$$

If the problem is geometry limited and $\mu_1 = \mu_2$

$$f = \frac{1}{3}\left[1 + \frac{2F}{cE}\mu_1\right] \tag{31}$$

This is the form of the Eddington factor in our code where E and F are the local energy density and flux, respectively. For the spherically symmetric imploding, burning pellet problem the material vacuum interface is not well defined. The radiation opacities vary much more slowly as a function

of radius. Thus, μ can not be defined in a unique way. To determine μ, the source function at the surface of a radiating sphere is assumed a linear function of the optical depth -- the Milne-Eddington model. For a sphere[24]

$$B_\tau = B_o \ (1 + 1.5 \ \tau) \ .$$

Consequently, at a point r, μ_1 is determined by the tangent drawn from r to a sphere, centered at the origin, and whose surface passes through a point two-thirds of a mean free path back along the radius from the point of interest, r.[13] Notice that as the mean free path becomes very large $F \to cE$ and $\mu \to 1$ and as the mean free path becomes very small $\mu_1 \to 0$. Thus, f limits to the correct physical values.

d. Multifrequency Group Averaging

Because the radiative mean free path is frequency dependent the first step in developing a numerical technique for solving the transport equation is to develop equations for frequency groups. To do this the range of frequencies must first be considered. This range is divided into a number of frequency groups (v_m, v_{m+1}) which can be changed to fit the conditions of the problem. To determine the transport equations for a given group the equations are integrated over the groups frequency range. For example, the transport equations for group (v_m, v_{m+1}) become

$$\frac{\partial E}{\partial t}(v_m) + \frac{1}{r^{\alpha-1}} \frac{\partial}{\partial r}(r^{\alpha-1} F(v_m) + c\bar{\sigma}_p(v_m) E(v_m) = J(v_m) \tag{32}$$

$$\frac{1}{c}\frac{\partial F}{\partial t}(v_m) + c\left[\frac{\partial}{\partial r} f(v_m) E(v_m) + \frac{\alpha-1}{2r}(3f(v_m) - 1) E(v_m)\right] + \bar{\sigma}_R(v_m) F(v_m) = 0 \tag{33}$$

where the various group averaged quantities are given by expressions of the form

$$A(v_m) = \int_{v_m}^{v_{m+1}} A(v)\, dv \ . \tag{34}$$

The Eddington factor for the group is

$$f(v_m) = \frac{1}{3}\left[1 + \frac{2F(v_m)}{cE(v_m)} \mu(v_m)\right] \ . \tag{35}$$

Notice that in order to do the frequency average of σ_a and $\sigma_a + \sigma_s$ F(v) and E(v) must be known, functions which are not known. Our approach is to assume a straight average in the energy equation,

$$\bar{\sigma}_p(v_m) = \frac{\int_{v_m}^{v_{m+1}} \sigma_a(v)\, dv}{\Delta v} \tag{36}$$

and a local Rosseland average in the flux equation.

$$\frac{1}{\bar{\sigma}_R(v_m)} = \frac{\int_{v_m}^{v_{m+1}} \frac{1}{(\sigma_a(v) + \sigma_s)} \frac{\partial B}{\partial T}(v, T)\, dv}{\int_{v_m}^{v_{m+1}} \frac{\partial B}{\partial T}(v, T)\, dv} \tag{37}$$

where T is the local electron temperature in the plasma and B(T,v) is the Planck distribution.

e. Boundary Conditions

The numerical calculation requires a value for the flux at both the right and left boundaries of the transport region. In our problems the outgoing flux needs to be calculated whereas the inner flux is assumed to be given. Consequently, the boundary flux has to be expressed in terms of the incoming flux and the radiation fields in the boundary zone. To accomplish this consider a simple problem. Consider a uniform temperature body whose surface is oriented symmetrically about the r axis, radiating into a vacuum region. The surface may be of any shape but since

one-dimensional geometry is assumed, the spherical surface shown in Figure 4 is chosen. Given an isotropic and steady-state source B, the radiation energy density E, flux F, and r-r component of the pressure tensor P are

$$E = \frac{2\pi B}{c}(1-\mu_1) \tag{38}$$

$$F = \pi B\,(1-\mu_1^2) \tag{39}$$

$$P = \frac{2\pi B}{3c}(1-\mu_1^3)\ . \tag{40}$$

since the radiation intensity is constant in the angular interval $\mu_1 \leq u \leq 1$. The u_1 can be determined by retardation or geometry. (Notice that a plane plasma surface would yield the same equations). Eqns. 38 and 40 give:

$$f = P/E = 1/3\,(1 + u_1 + u_1^2)$$

and $$F/E = c/2\,(1 + \mu_1)\ .$$

Thus, $$f = 1/3\,(1 - \frac{2F}{cE} + (\frac{2F}{cE})^2) \tag{41}$$

Solving this equation for F yields:

$$F = scE \text{ where} \tag{42}$$

$$s = 1/2\,(1 + \sqrt{1 + 4(3f-1)})\ . \tag{43}$$

The total energy density and flux at the right boundary can be written as

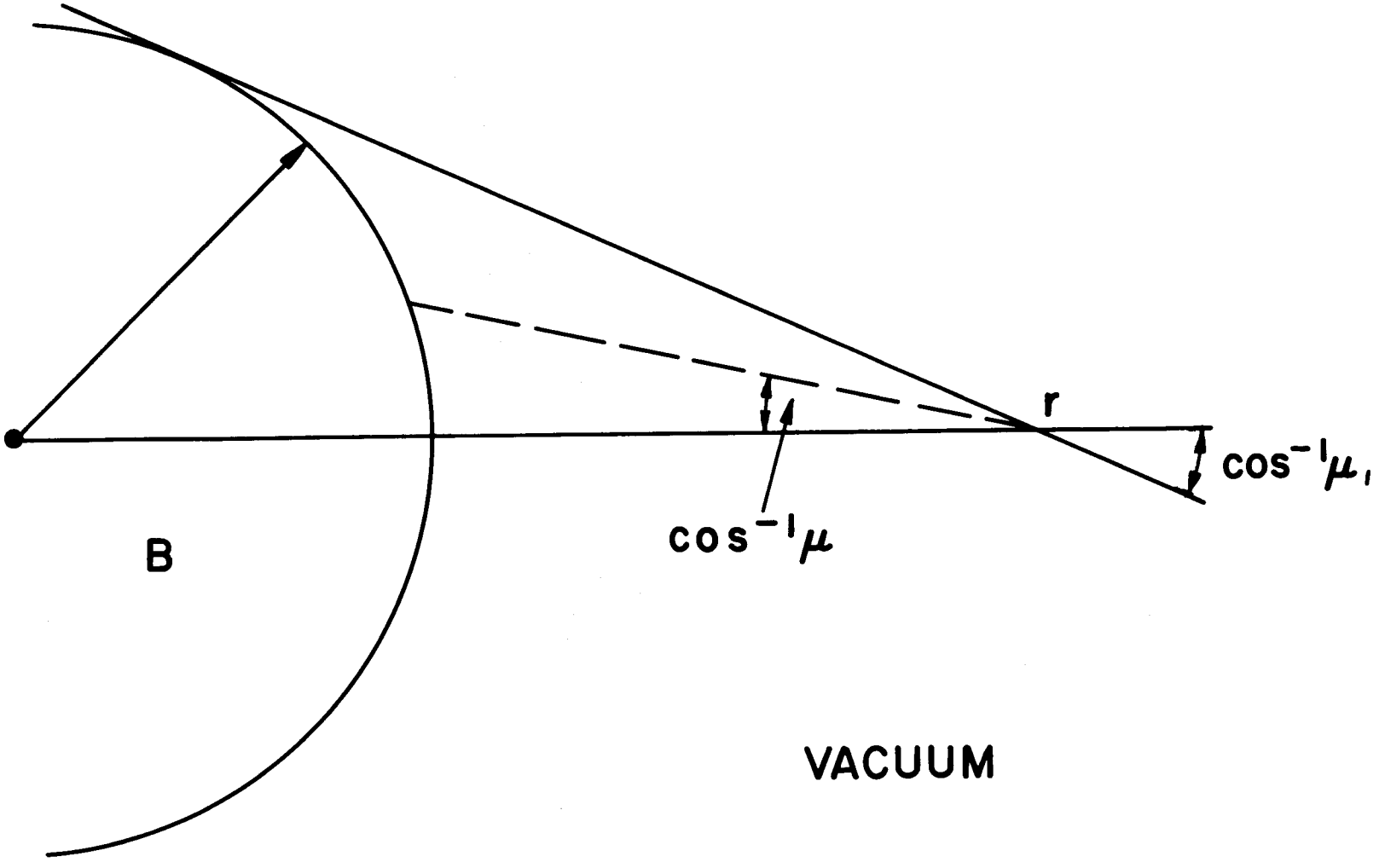

FIG. 4 ISOTHERMAL SPHERE, μ_1, GEOMETRY LIMITED

$$E = 1/c \int_0^1 I_+ \, d\mu + 1/c \int_{-1}^0 I_- \, d\mu \qquad (44)$$

$$F = \int_0^1 I_+ \, \mu d\mu + \int_{-1}^0 I_- \, \mu d\mu \qquad (45)$$

where the incoming flux $F_- = \int_{-1}^0 I_- \, \mu d\mu$ and the outgoing flux $F_+ = \int_0^1 I_+ \, \mu d\mu$.

Using Eqns. 44 and 45 the total flux can be written as

$$F = cE/2 - 2F_- \, . \qquad (46)$$

If the incoming is assumed much less than the outgoing radiation, for isotropic outgoing radiation $E \tilde{-} I_+/c = 2 F_+/c$. From the previous problem $F_+ = scE$ where E is the radiation energy density at the boundary. Thus, at the right boundary, $F_R = scE - 2 F_-$.(47) A similar calculation yields an equation for the total flux at the left boundary. It is

$$F_L = -scE + 2F_+ \, . \qquad (48)$$

For spherically symmetric geometry $F_L = 0$.

f. Radiation Coupling to the Ions and Electrons

In modeling the time evolution of an imploding, burning pellet, it is necessary to solve the coupled ion, electron and radiation equations. Because a two-temperature, one-fluid hydrodynamical model for the ion and electron motion is used, the electron internal energy equation is given by

$$\frac{d\varepsilon_e}{dt} = - P_e \frac{dv}{dt} - \frac{c_v^i}{\tau} (T_e - T_i)$$

$$+ \frac{1}{\rho\, r^{\alpha-1}} \frac{\partial}{\partial r} (K_e\, r^{\alpha-1} \frac{\partial Te}{\partial r}) +$$

$$1/\rho \sum_k (c\, \sigma_p(v_k)\, E(v_k) - J(v_k)) + \dot{S}_e \quad (49)$$

where ε_e is the electron internal energy per unit mass, P_e is the electron partial pressure, C_v^i is the ion specific heat, K_e is the electron thermal conductivity, τ is the electron -- ion collision exchange time, $1/\rho \sum_k (c\, \sigma_p(v_k)\, E(v_k) - J(v_k))$ are the radiation energy emission and absorption terms and $\dot{S}_e$ is the energy source term due to laser coupling and thermonuclear burn. Radiation is also coupled to the electron and ion fluid motion through the radiation pressure.

The computer code is written to do any one of three different treatments of the radiation transport problem. A time independent frequency dependent problem can be solved. For example, to do this calculation the time derivatives in the multifrequency equations are ignored and the absorption and emission terms given on the hydrodynamic time scale are used. A frequency independent time dependent calculation, i.e., the one frequency group case can be done. A frequency dependent time dependent calculation which doesn't require the solution to the coupled set of ion, electron and multifrequency radiation equations can also be performed.[13] This is accomplished by first doing a frequency dependent time independent

calculation for the energy density, flux and pressure. With these calculated variables frequency-averaged values of the absorption coefficients and Eddington factors are found. These calculated averaged values are then used to do a frequency averaged time dependent calculation of the energy and flux and the averaged energy density and flux are coupled to the ion and electron energy and the fluid motion. By doing this the coupled multigroup radiation, ion and electron energy equations are replaced with coupled one group radiation, ion and electron equations. This fact could greatly reduce the computer cost.[13] A detailed description of the numerical techniques for the methods described here will be given in a later report.

g. Spectral Information

To make the hydro-burn calculation with radiation transport economic as few frequency groups as possible are employed - the number of groups being determined by whether or not the temperature and density history of the plasma can be found accurately enough. On the other hand, the X-ray spectral structure should be determined. To meet the latter requirement a post-processing large multifrequency time independent radiation calculation can be done. For example, this time independent calculation could be done with 20 to 40 frequency groups whereas the implosion and burn calculation would be done with as few as 10 groups.

VI. Tamped Pellets

a. Introduction

This section is divided into three parts. The first gives a brief description of the calculated radiation results. No attempt is made to describe the results physically. In the second a chronological description of burn evolution is used to focus the reader's attention on the important interconnected hydrodynamic, burn dynamic and radiation processes suggested by our calculations. Lastly, our results are compared with other calculations found in the literature.

b. Results

Since one of our goals was to gain an estimate of how fractional burnup and X-ray spectra change with tamper mass, absorption and implosion effects were ignored. Consequently, our calculations began with a compressed core of DT. In all calculations except one the DT was surrounded by a layer of mercury. For the results displayed in Table I, the initial number density (electron and ion) was uniform (1.61×10^{26} cm^{-3}) throughout and the temperature was 10 keV at the center of the DT and .136 keV everywhere else. Table II displays similar calculations except that the initial mercury density was not uniform. In the latter case, pressure balance was assumed in the core contact region but the mercury density decreased as $1/r^3$ thereafter. Since these are strictly model calculations with no justification for the density configuration at burn start it was felt that these two models would be sufficiently different to span the range of density profiles. These qualitative results suggest that a mercury mass exists for maximizing the conversion of energy to X-rays for both of the postulated density profiles. They also suggest that the fractional burnup tends to increase as the mercury mass is increased.

Table I

DT (mg)	Hg (mg)	X-rays		Charged Particles		Neutrons		Total Energy
		MJ	%	MJ	%	MJ	%	MJ
1	0.0	1	1	20	19.4	82	79.6	103
1	2	14	.8	21	12	142	80	177
1	10	23	10	23	10	191	80	237
1	50	18	6	41	14	237	80	296

Table II

DT (mg)	Hg (mg)	X-rays		Charged Particles		Neutrons		Total Energy
		MJ	%	MJ	%	MJ	%	MJ
1	10	23	10	22	10	187	80	232
1	50	28	11	23	9	205	80	256
1	100	25	10	25	10	203	80	253

Fig. 5 shows time plots of the X-ray energy leaving the pellet surface for the four cases given in Table I. The corresponding time plots for the calculations given in Table II yield similar characteristics. Figures 6 to 10 display the time-integrated X-ray spectra approximately 2 nsec after burn starts. These results suggest that both the X-ray transit time and spectra are significantly altered by the amount of high Z material in the pellet. For example, the results indicate that the width of the X-ray energy time pulse to the wall is greatly increased and the X-ray spectra significantly altered when the mercury mass is increased and when the density profile is altered.

c. Discussion

Because these calculations were done for a specific high Z material and for special initial conditions, it is of interest to explore some of the more general qualitative physical processes suggested by our calculation. By focussing on the more important interconnected hydrodynamic, burn dynamic and radiation processes occurring during and after burn, some understanding of the previous results and some qualitative understanding of more complex pellet designs can be made.

Consider the radiation processes within a DT pellet surrounded by a high Z material. When burn starts the temperature of the DT significantly rises and with this increase comes a corresponding increase in the radiation energy density. As the burn develops, radiation penetrates the high Z layer. If the high Z shell is sufficiently thick and dense the radiation is absorbed and most reemitted back into the DT. The radiation becomes trapped.

At the same time a thermal conduction wave begins propagating through the high Z material. As the wave propagates outward the high Z layer becomes

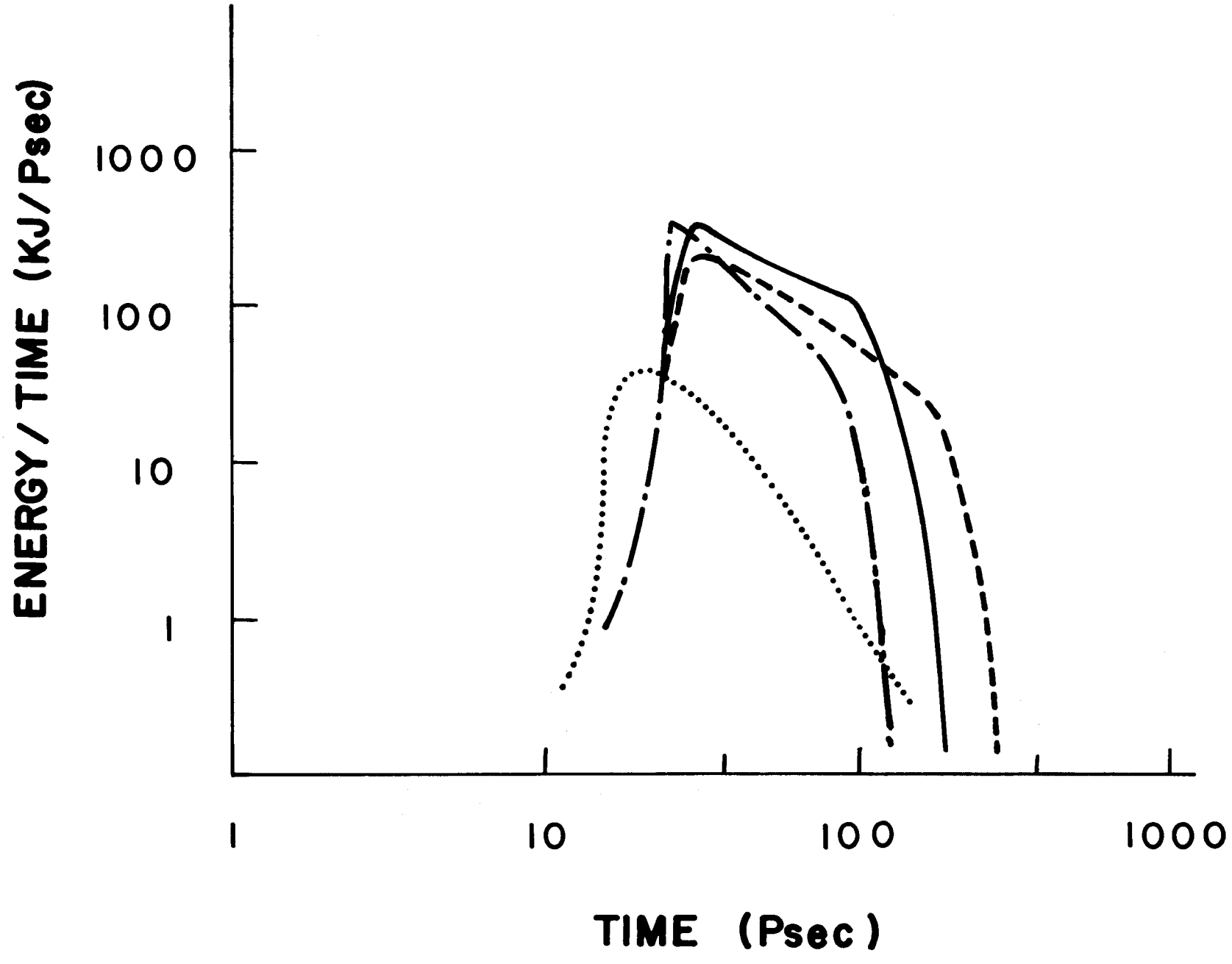

FIG. 5 RADIATION ENERGY LEAVING THE PELLET'S SURFACE.
THE CURVES REFER TO THE FOLLOWING CASES: BARE DT (DOTTED), 2mg OF Hg (DASH-DOT), 10 mg OF Hg (SOLID) AND 50mg OF Hg (DASH).

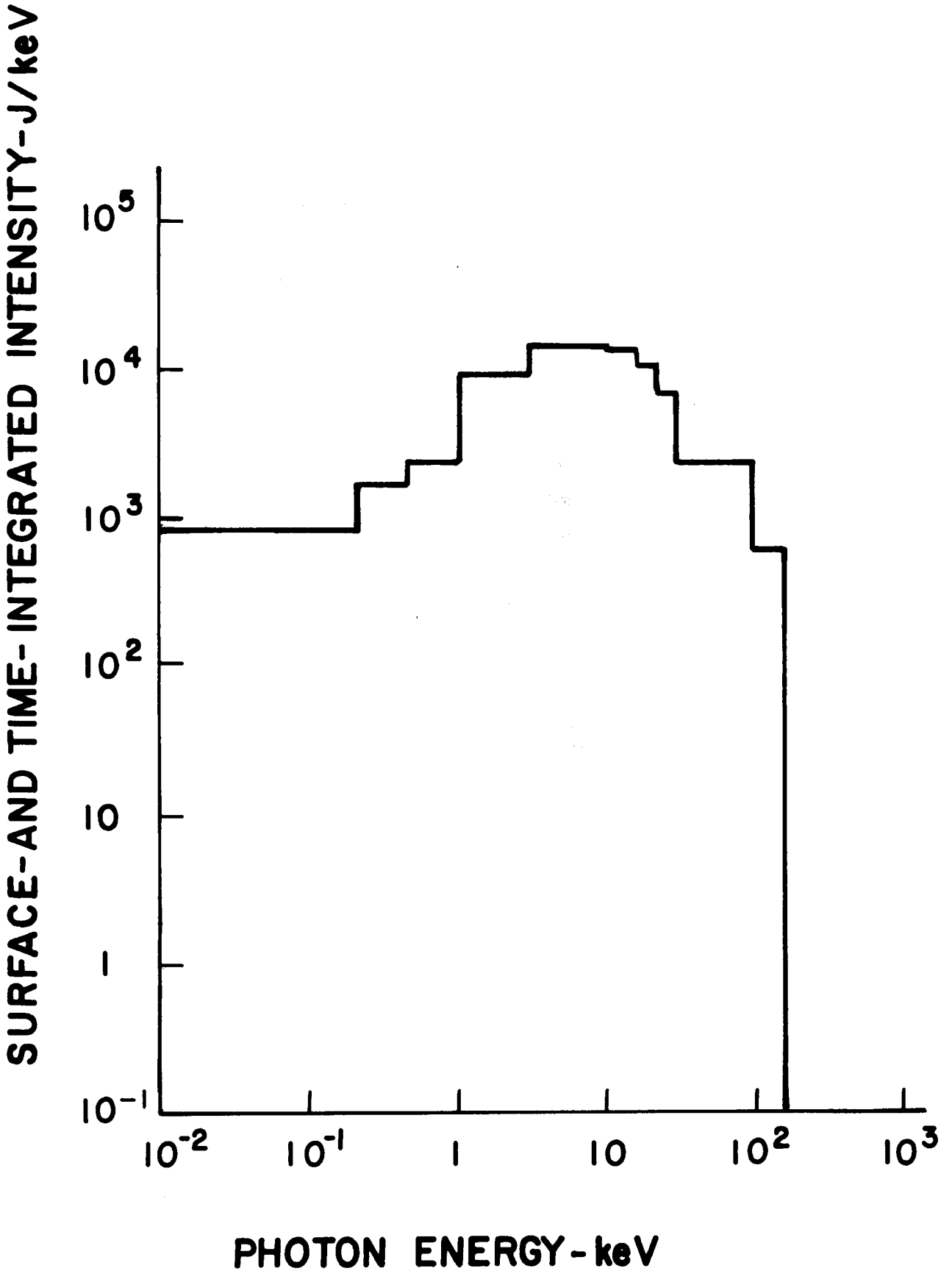

FIG. 6 RADIATION SPECTRUM FOR BARE DT PELLET. (10 FREQUENCY GROUPS)

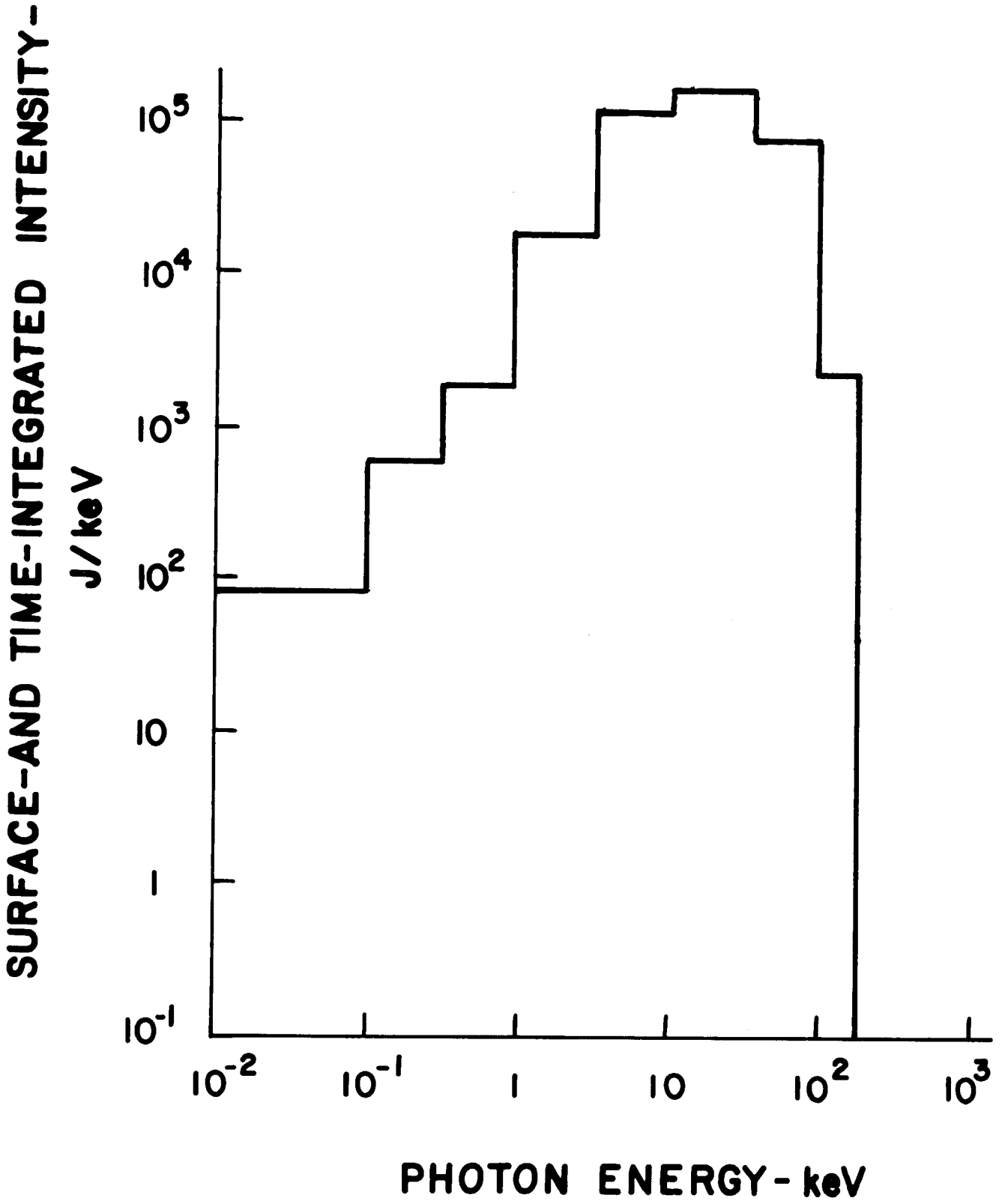

FIG. 7 RADIATION SPECTRUM FOR A DT PELLET WITH A 2 mg Hg SHELL.

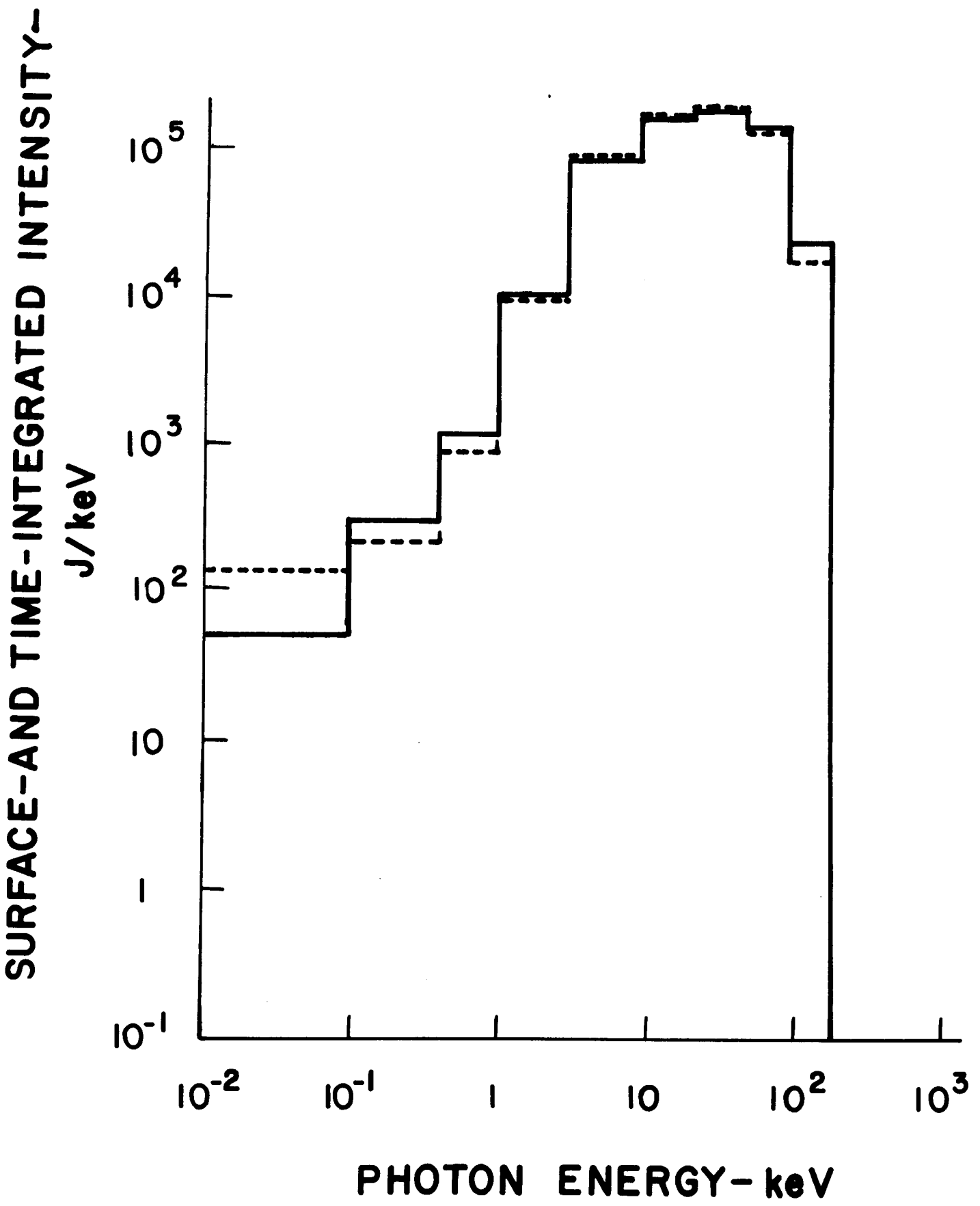

FIG. 8 RADIATION SPECTRUM FOR A DT PELLET WITH A 10 mg Hg SHELL. (SOLID CURVE ASSUMED UNIFORM Hg DENSITY)

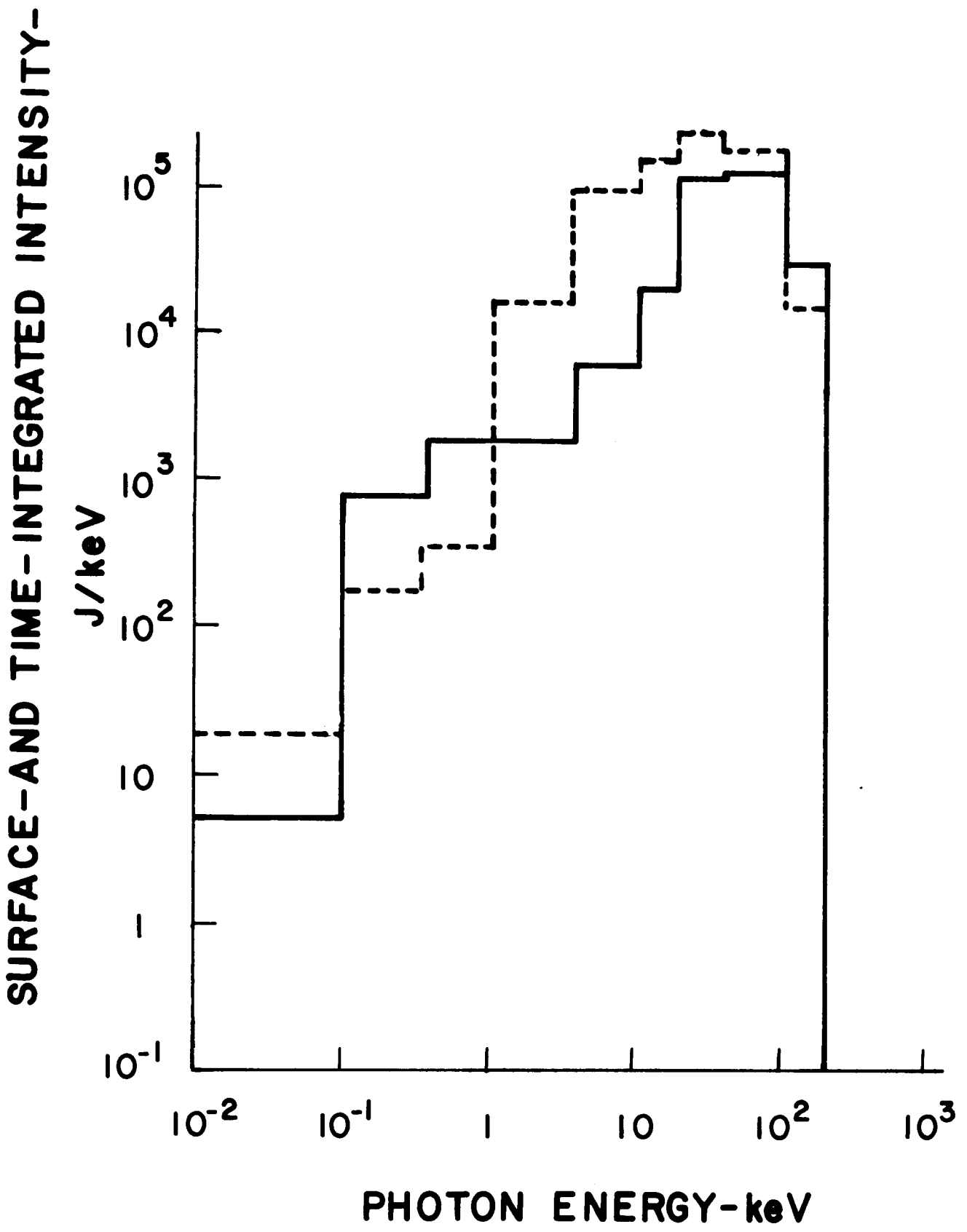

FIG. 9 RADIATION SPECTRUM FOR A DT PELLET WITH A 50 mg Hg SHELL. (SOLID CURVE ASSUMED UNIFORM Hg DENSITY)

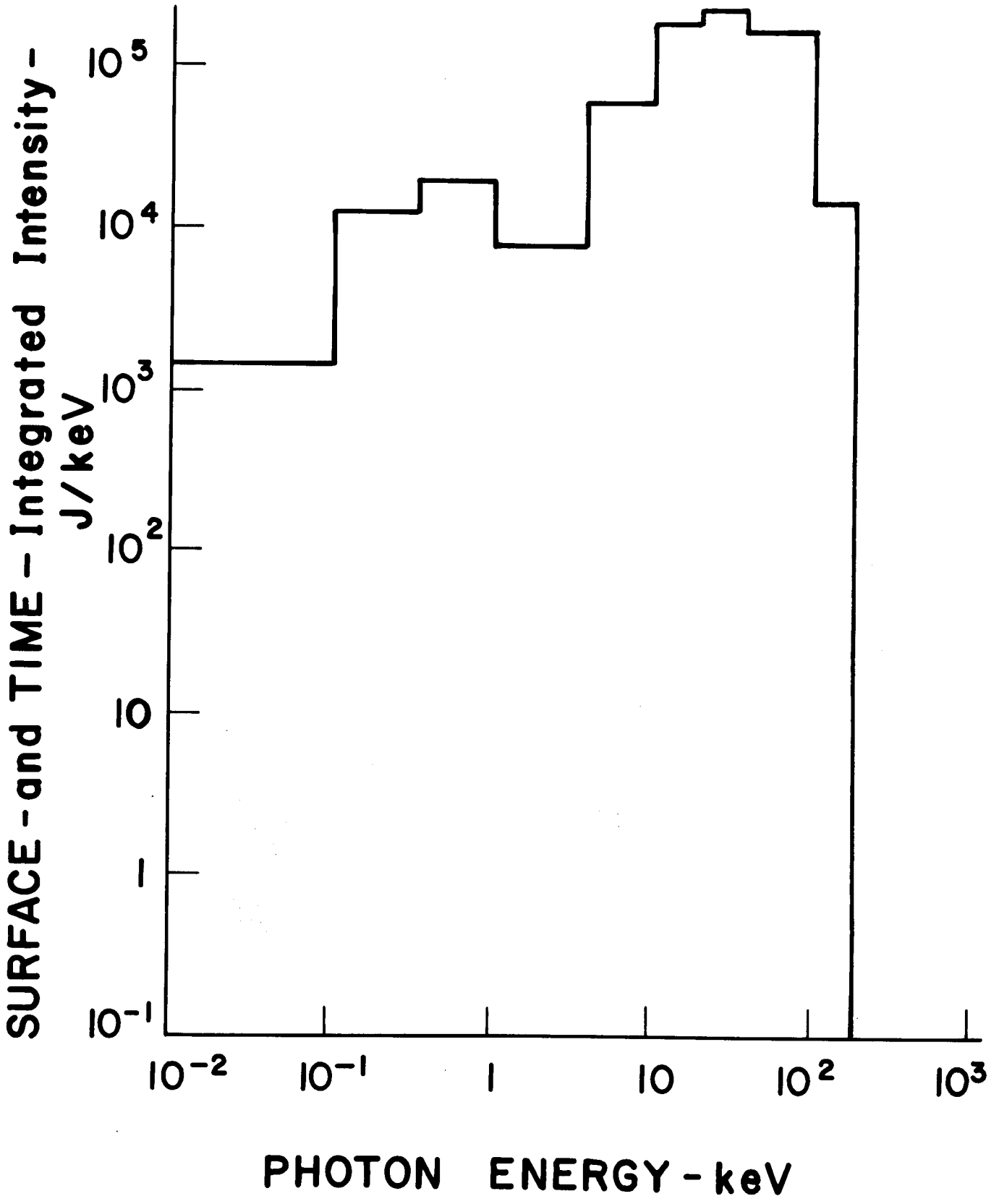

FIG 10 RADIATION SPECTRUM FOR A DT PELLET WITH A 100 mg Hg SHELL

more ionized. The ionization state changes the radiation emission, absorption and scattering functions and, therefore, the radiation transport. For example, the absorption process for a highly ionized high Z layer will tend to be inverse bremsstrahlung at low frequencies and photoelectric absorption at high frequencies. The emission will increase as the temperature increases. Further, if the energy released during burn significantly ionizes the high Z layer, the pellet may become transparent to much of the radiation and the surface-emitted-X-rays will tend to be hard. In contrast, if the energy released is small compared to the amount needed to significantly ionize the layer, radiation mean free paths will remain small and the surface-emitted-X-rays will tend to be soft.

As the conduction wave propagates outward, the inner surface of the high Z layer ablates inward. The ablation process will impart more momentum to the shell if the penetration depth of the DT debris is small compared to the shell's thickness. For example, if the debris is stopped in the inner surface of the shell, the pressure of the inner surface rises considerably because both its temperature and ionization state are rapidly increasing. As a result, much of the debris energy is converted into momentum. On the other hand, if the DT debris penetrates deeply into the high Z layer, the shell is heated without substantial conversion of energy into momentum.

Because a conduction wave increases the plasma temperature and, therefore the radiation emission, and because radiation tends to flow outward rather than inward from the pellet's surface, radiation cooling increases when the conduction wave reaches the pellet's surface. For low energy photons, radiation loss is generally a surface effect because the photon

mean free path is small. On the other hand, because high energy photons tend to have much larger mean free paths, hard X-rays from the DT burning core and from the inner surface of the mercury shell may reach the pellet surface without substantial absorption.

The pellet density structure during and after burn completion will significantly affect the total radiation energy and momentum of the pellet debris and the resulting radiation spectrum. If the inner DT and high Z layer collide with a massive lower density outer layer of ablated pellet material, some kinetic energy of the inner layer is lost in the process of heating the lower density outer region. The outer layer then radiates away much of this increased thermal energy. As the pellet expands outward, more thermal energy is transferred into particle kinetic energy and low energy photons, and ionization recombination increases both the electron thermal and radiation energies.

Concluding, our results suggest the following pellet characteristics. If two pellets with equal DT but different high Z masses are brought to a similar ignition condition, the pellet with the larger high Z mass will tend to produce softer X-rays, lower particle energies and longer X-ray transit times. Further, the greater the high Z compression achieved during implosion and the greater the amount of high Z mass compressed, the smaller the X-ray energy content. Finally, again consider two pellets, with equal DT but different high Z masses which are brought to a similar ignition condition. Because the pellet disassembly is slowed more for the higher mass pellet, the larger mass pellet will tend to have a higher fractional burnup.

d. A Comparison With Published Results

Before the radiation transport code was integrated into the hydrodynamic-burn code, a comparison of our radiation treatment with the calculations of Apruzese and Davis[15] was made. Fig. 11 indicates the good agreement between their calculations and ours for some simple problems. In Fig. 11, J is the mean radiation intensity defined as

$$J = 1/2 \int_{-1}^{1} I(\mu)d\mu$$

where $I(\mu)$ is the specific intensity and where μ is the angle between the direction of radiation flow and the radial direction-spherical symmetry is assumed. For the three problems shown, the source function defined as the emission coefficient divided by the absorption coefficient was constant. The three cases considered were kR_0 = 1.3, 4.9 and 100 where k is the absorption coefficient and where R_0 is the radius of the sphere.

With the radiation included in the PHD-IV hydrodynamics-burn code, we reproduced the X-ray spectrum from a burning bare DT pellet core, computed at Lawrence Livermore Laboratory, presumably by LASNEX.[16] This comparison is shown in Fig. 12 and again we are in very good agreement. Our partition of total energy between X-rays (1%) and charged particles (20%) is also in good agreement.

A far more severe test of our code is the comparison of X-ray spectra with an e-beam pellet calculation the results of which are contained in a paper by Varnado and Carlson.[17] This pellet contained approximately 200 mg of gold surrounding the DT. To make this comparison, a gold density profile was chosen to model the state of the plasma just before ignition.

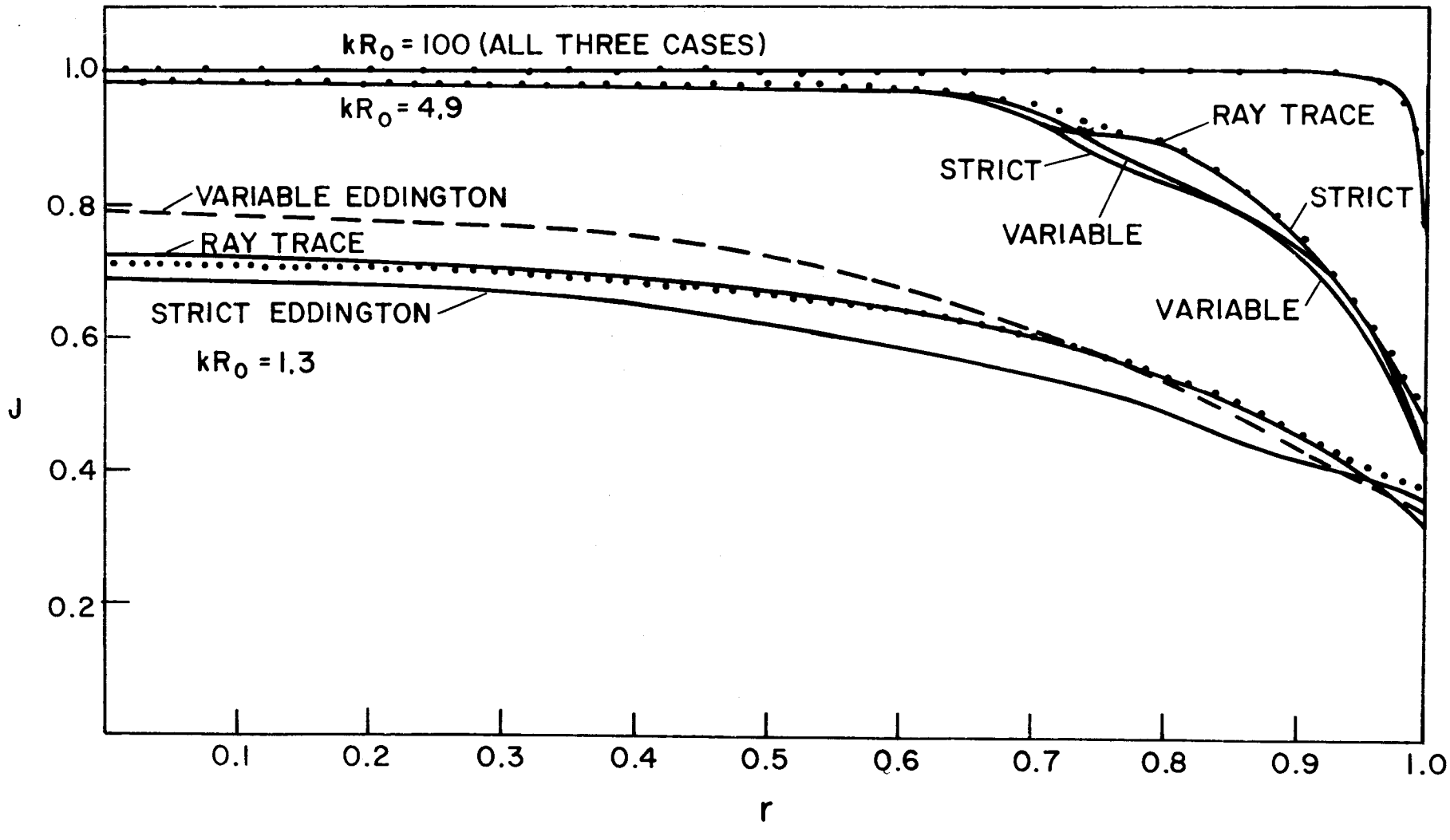

Fig. 11 Mean intensity J vs. radius r for optical depths of 1.3, 4.9 and 100 for ray-trace, strict Eddington and variable Eddington transport calculations (dotted lines give our calculations).

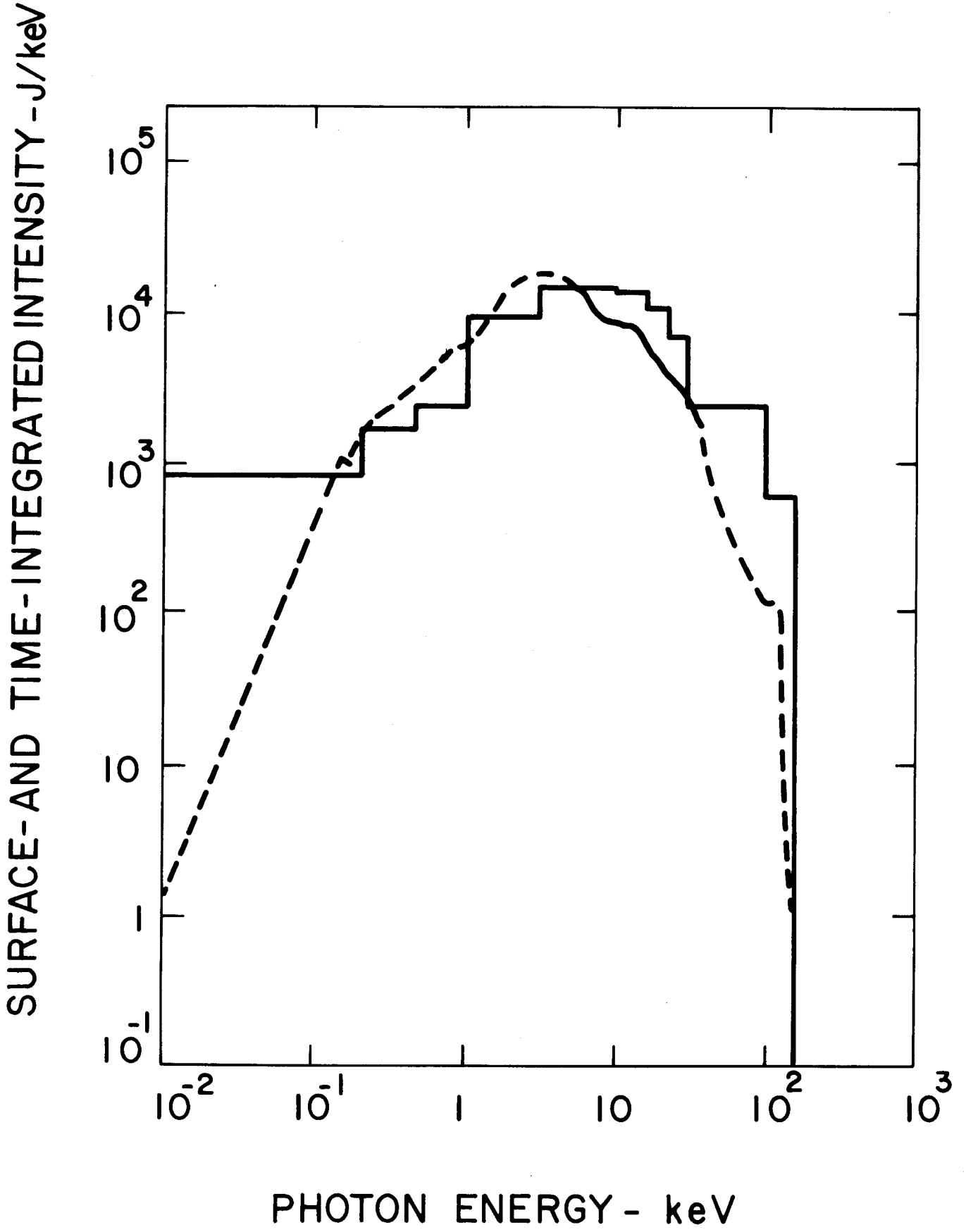

Fig. 12 Radiation spectrum for bare DT pellet (dashed curve is Livermore spectrum scaled to a 100 MJ yield)

The gold density decreased as $1/r^3$ for the first 100 mg and was constant thereafter. The DT was assumed to be at a constant density and the DT and Au pressures were matched to be equal at their interface. Fig. 13 shows the resulting X-ray spectrum at 12 nsec after ignition. The soft portion of the spectrum is in relatively good agreement with the results in Ref. 17 for a 350 eV black-body. The hard portion of our spectra results from the non-LTE nature of our radiation transport calculation. However, our calculations only include bremsstrahlung emission and inverse bremsstrahlung absorption processes. If one includes photoelectric absorption and incoherent scattering processes, this hard component of the spectrum may disappear. If we ignore the hard portion, the radiation flux peaks at about 9 nsec after ignition and decays on a time scale similar to the rise time in agreement with the results of Clauser.[17] The total photon energy emitted is approximately 4 MJ (5%), the neutron energy about 61 MJ and the charged particle energy about 11 MJ (15%).

VII. Comments

A very simple model of radiation emission and absorption was used in the calculations presented, i.e., we assumed bremsstrahlung emission and inverse bremsstrahlung absorption. Bound-bound and bound-free emission and their absorption counterparts will become more and more important as the amount of high Z mass around the pellet is increased. As the mass of the high Z material is increased, the addition of bound-bound and bound-free processes will significantly decrease the high energy photon mean free path. Thus, for example, if these processes were included in our calculations for the 50 and 100 mg simulations with mercury, the surface integrated X-ray spectra for these cases would lack a portion of the hard X-rays.

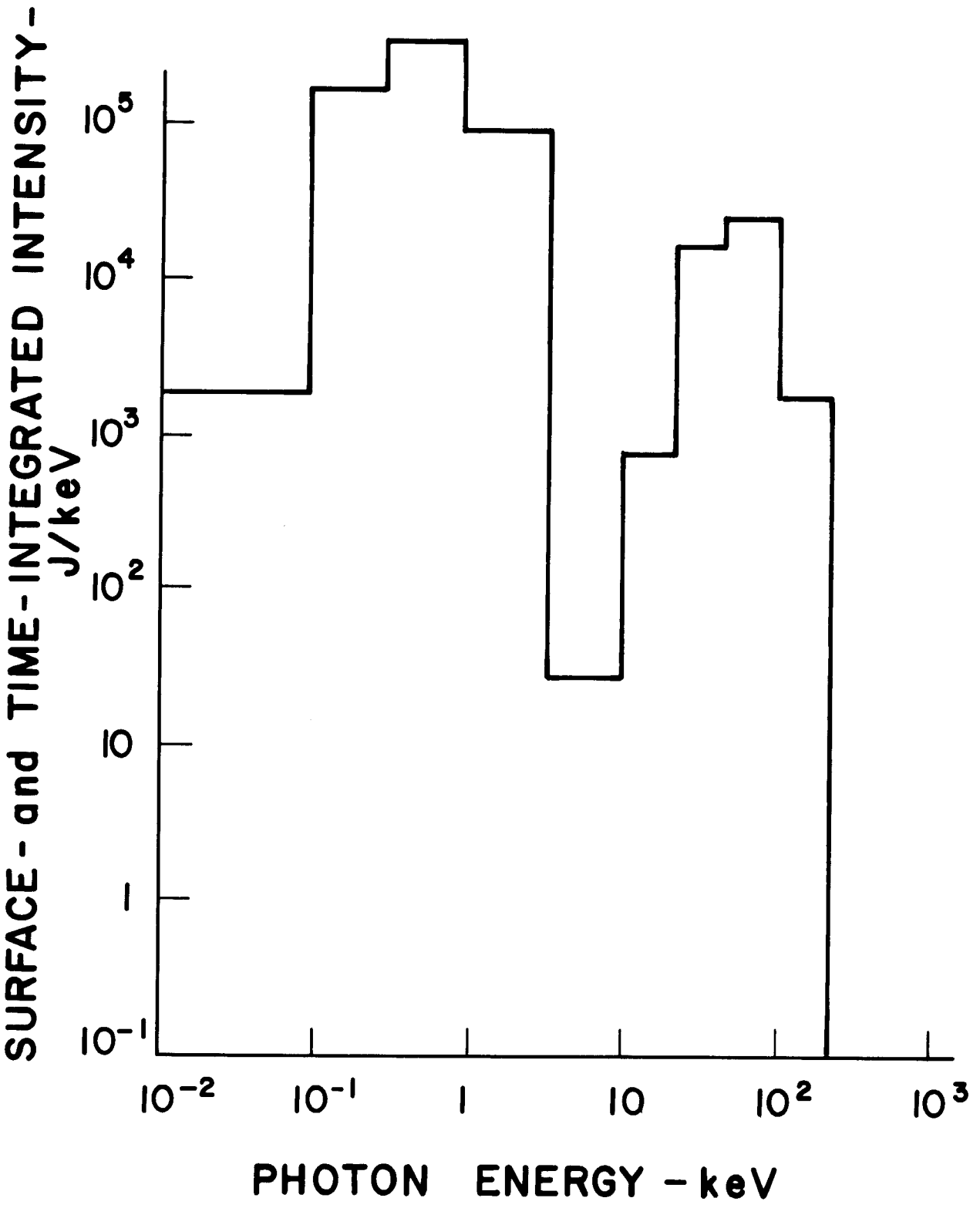

FIG. 13 RADIATION SPECTRUM FOR A DT PELLET WITH A 200 mg AU SHELL

The thermonuclear burn time is short compared to the time it takes some pellets to disassemble. For example, for the pellets with 10 mg of mercury discussed in the last section this is true. The transit time, the time it takes a 14 MeV neutron to travel through the pellet, is also much less than the disassembly time. Further, the mean free path of a neutron is large by pellet dimensions. For the above reasons it is likely that neutron energy loss within the pellet will initially more effectively heat rather than increase the plasma kinetic energy. This increased heating will increase the radiation energy density and the radiation losses from the pellet surface. Thus, the total percentage of X-rays lost by the pellet will increase as the neutron energy loss increases.

It was suggested in an earlier section that collective effects may have to be included in an analysis of alpha particle transport. If the net effect of collective fields is to increase the slowing down of alpha particles, this slowing could be advantageous in at least a couple of ways. This increased slowing down will give rise to higher temperatures. These higher temperatures increase the possibility of the D-D reaction and increase the radiation energy density. The increase in radiation energy could be exploited in the following way. If the DT contain a homogeneous and small portion of high Z material, radiation will be more effectively absorbed and trapped than in the pure DT case. In addition, through scattering and absorption the radiation could act an an effective electron heat source. Thus, for example, if the radiation energy content is large enough one might be able to create a radiation burn wave. If the radiation energy content is not large enough for this to happen, radiation transport could still play a significant role. For example, because

radiation will transport energy more quickly than alpha particles, the disassembly will likely be slowed by radiation transport because fluid pressure gradients will be reduced.

This section may not have been very satisfying to the reader since it contains much conjecture. However, we feel justified by this conjecture because our purpose here is to suggest important areas which we think need further study and to suggest some of the consequences of these studies to initiate interest.

References

1. J. Nuckolls, et al., "Laser Compression of Matter to Super-High Densities: Thermonuclear Applications", Nature 239, 139-142 (1972).

2. P. M. Campbell, et al., "Radiation Processes in a Laser-Fusion Plasma", KMSF-V457 (1976).

3. K. Brueckner and S. Jorna, Rev, Mod. Phys. 46, 325 (1974).

4. S. Chapman and T. Cowling, The Mathematical Theory of Non-Uniform Gases, (Cambridge University Press, Cambridge, 1953).

5. Landau and Liftsitz, Statistical Physics, 2nd Ed., (Addision-Wesley, Reading, Mass., 1969).

6. S. G. Brush, in Progress in High Temperature Physics and Chemistry, Vol. I, Ed. C. A. Rouse (Pergamon Press, London, 1967).

7. L. Spitzer, Physics of Fully Ionized Gases, (Wiley, New York, 1965).

8. J. Shearer, UCID-15745, 1970.

9. J. Von Neumann, J. Appl. Phys. 21, 232 (1950).

10. K. Brueckner and H. Brysk, J. Plasma Phys. 10, 141 (1973).

11. G. C. Pomraning, Radiation Hydrodynamics, Pergamon Press, Oxford (1973).

12. S. I. Pai, Radiation Gas Dynamics, Springer-Verlag (1966).

13. P. M. Campbell and J. J. Kubis, "A Variable Eddington Method for Radiation Transport in Dense Fusion Plasmas", KMSF-U458 (1976).

14. P. M. Campbell, "A Numerical Method for Discrete Ordinate and Moment Equations in Radiation Transfer", Int. J. Heat Mass Transfer 12, 497 (1969).

15. J. P. Apruzese and J. Davis, "Evaluation of the Radiation Field in a Spherically Symmetric Plasma, "NRL Memorandum Report 3277 (1976).

16. J. Hovingh, J. Maniscalco, M. Peterson and R. Werner, "The Preliminary Design of a Suppressed-Ablation, Laser Reduced Fusion Reactor", Lawrence Livermore Lab. Report UCRL-75368 (1973).

17. S. Varnado and G. Carlson, Nucl. Tech. 29, (1976).